



King's Research Portal

DOI:

[10.1016/j.ymthe.2018.10.006](https://doi.org/10.1016/j.ymthe.2018.10.006)

Document Version

Publisher's PDF, also known as Version of record

[Link to publication record in King's Research Portal](#)

Citation for published version (APA):

Man, F., Lim, L., Volpe, A., Gabizon, A., Shmeeda, H., Draper, B., Parente-Bergreira, A. C., Maher, J., Blower, P. J., Fruhwirth, G. O., & T.M. de Rosales, R. (2019). *In Vivo* PET Tracking of ⁸⁹Zr-Labeled V9V2 T Cells to Mouse Xenograft Breast Tumors Activated with Liposomal Alendronate. *Molecular Therapy*, 27(1), 219-229. <https://doi.org/10.1016/j.ymthe.2018.10.006>

Citing this paper

Please note that where the full-text provided on King's Research Portal is the Author Accepted Manuscript or Post-Print version this may differ from the final Published version. If citing, it is advised that you check and use the publisher's definitive version for pagination, volume/issue, and date of publication details. And where the final published version is provided on the Research Portal, if citing you are again advised to check the publisher's website for any subsequent corrections.

General rights

Copyright and moral rights for the publications made accessible in the Research Portal are retained by the authors and/or other copyright owners and it is a condition of accessing publications that users recognize and abide by the legal requirements associated with these rights.

- Users may download and print one copy of any publication from the Research Portal for the purpose of private study or research.
- You may not further distribute the material or use it for any profit-making activity or commercial gain
- You may freely distribute the URL identifying the publication in the Research Portal

Take down policy

If you believe that this document breaches copyright please contact librarypure@kcl.ac.uk providing details, and we will remove access to the work immediately and investigate your claim.

In Vivo PET Tracking of ^{89}Zr -Labeled $\text{V}\gamma 9\text{V}\delta 2$ T Cells to Mouse Xenograft Breast Tumors Activated with Liposomal Alendronate

Francis Man,¹ Lindsay Lim,¹ Alessia Volpe,¹ Alberto Gabizon,² Hilary Shmeeda,² Benjamin Draper,³ Ana C. Parente-Pereira,³ John Maher,³ Philip J. Blower,¹ Gilbert O. Fruhwirth,¹ and Rafael T.M. de Rosales¹

¹School of Biomedical Engineering & Imaging Sciences, King's College London, St Thomas' Hospital, London SE1 7EH, UK; ²Oncology Institute, Shaare Zedek Medical Center and Hebrew University–School of Medicine, Jerusalem 9103102, Israel; ³School of Cancer and Pharmaceutical Sciences, King's College London, Guy's Hospital, London SE1 9RT, UK

Gammadelta T ($\gamma\delta$ -T) cells are strong candidates for adoptive immunotherapy in oncology due to their cytotoxicity, ease of expansion, and favorable safety profile. The development of $\gamma\delta$ -T cell therapies would benefit from non-invasive cell-tracking methods and increased targeting to tumor sites. Here we report the use of [^{89}Zr]Zr(oxinate)₄ to track $\text{V}\gamma 9\text{V}\delta 2$ T cells *in vivo* by positron emission tomography (PET). *In vitro*, we showed that ^{89}Zr -labeled $\text{V}\gamma 9\text{V}\delta 2$ T cells retained their viability, proliferative capacity, and anti-cancer cytotoxicity with minimal DNA damage for amounts of $^{89}\text{Zr} \leq 20$ mBq/cell. Using a mouse xenograft model of human breast cancer, ^{89}Zr -labeled $\gamma\delta$ -T cells were tracked by PET imaging over 1 week. To increase tumor antigen expression, the mice were pre-treated with PEGylated liposomal alendronate. Liposomal alendronate, but not placebo liposomes or non-liposomal alendronate, significantly increased the ^{89}Zr signal in the tumors, suggesting increased homing of $\gamma\delta$ -T cells to the tumors. $\gamma\delta$ -T cell trafficking to tumors occurred within 48 hr of administration. The presence of $\gamma\delta$ -T cells in tumors, liver, and spleen was confirmed by histology. Our results demonstrate the suitability of [^{89}Zr]Zr(oxinate)₄ as a cell-labeling agent for therapeutic T cells and the potential benefits of liposomal bisphosphonate treatment before $\gamma\delta$ -T cell administration.

INTRODUCTION

Adoptive transfer of therapeutic T cells is a growing field in immunoncology, with spectacular clinical results against melanoma and hematological cancers.^{1–3} Gammadelta-T ($\gamma\delta$ -T) cell therapy is one type of T cell therapy being explored, with recent data showing intra-tumoral $\gamma\delta$ -T cells are the single most favorable prognostic immune cell infiltrate.⁴ $\gamma\delta$ -T cells perform roles belonging to both adaptive and innate immunity, playing a significant role in anti-infectious and anti-tumor immune surveillance.⁵ Activated $\gamma\delta$ -T cells are highly cytotoxic, enhance the function of other immune cells, and act as antigen-presenting cells.⁶ In humans, the $\text{V}\gamma 9\text{V}\delta 2$ subtype of $\gamma\delta$ -T cells represents 1%–5% of circulating CD3⁺ T cells.⁶ Their potent cytotox-

icity and high proliferative capacity have made them candidates of choice for cancer immunotherapy.⁷

The unique activation of $\text{V}\gamma 9\text{V}\delta 2$ cells by phosphoantigens such as isopentenyl pyrophosphate (IPP)⁸ allows them to discriminate between normal and metabolically disordered cells based on IPP expression levels.⁹ The activation and targeting of $\gamma\delta$ -T cells to tumor tissue could, therefore, be improved by selectively increasing the presentation of phosphoantigens in cancer cells, for example, by using liposome- or nanocarrier-based formulations of aminobisphosphonate drugs (NBPs).¹⁰ NBPs (e.g., pamidronate, alendronate, and zoledronate),¹¹ which increase the expression of IPP in target cells by inhibiting farnesyl diphosphate synthase, are hydrophilic molecules that accumulate in bone, but not in other tissues, and are rapidly cleared from the circulation. Encapsulating alendronate in liposomes has been shown to increase the therapeutic efficacy of $\gamma\delta$ -T cells in preclinical models.^{12,13}

Clinical studies of $\gamma\delta$ -T cell immunotherapy have shown a good safety profile and efficacy comparable to second-line anticancer therapies, but they have also highlighted the need for improvements.^{14,15} Unknown aspects of adoptive $\gamma\delta$ -T cell therapy include their *in vivo* distribution and kinetics of arrival at the tumor site. Whole-body imaging is highly useful in this context by enabling *in vivo* tracking of administered cells. Many techniques exist for non-invasive cell tracking,^{16–18} however, only nuclear imaging, and particularly positron emission tomography (PET), provides sensitive and quantitative, whole-body information with adequate spatiotemporal resolution. Hence, methods to radiolabel and track therapeutic cells using positron-emitting radionuclides are likely to become important tools for cell immunotherapy.¹⁹

Received 5 June 2018; accepted 8 October 2018;

<https://doi.org/10.1016/j.ymthe.2018.10.006>.

Correspondence: Rafael T.M. de Rosales, PhD, School of Biomedical Engineering & Imaging Sciences, King's College London, St Thomas' Hospital, Westminster Bridge Road, London SE1 7EH, UK.

E-mail: rafael.torres@kcl.ac.uk



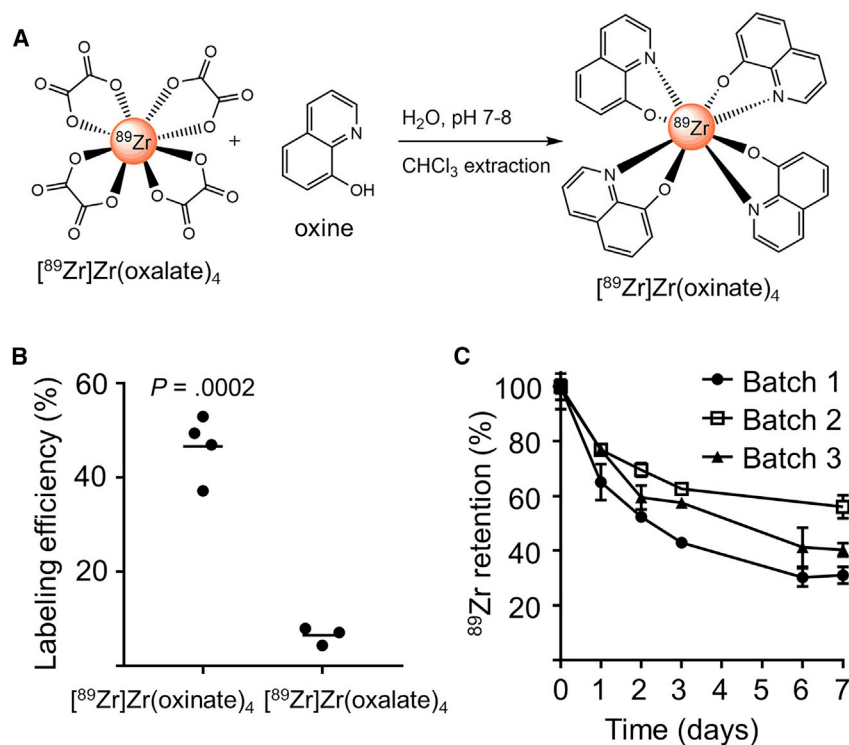


Figure 1. Radiotracer Synthesis and $\gamma\delta$ -T Cell Radiolabeling

(A) $[^{89}\text{Zr}]\text{Zr}(\text{oxinate})_4$ synthesis. (B) Labeling efficiencies of $\gamma\delta$ -T cells incubated with ^{89}Zr -based tracers (63.2 ± 7.9 mBq/cell) 20 min at RT. Mean of $N = 3$ –4 individual experiments (unpaired t test). (C) ^{89}Zr retention by $\gamma\delta$ -T cells over 7 days after labeling with $[^{89}\text{Zr}]\text{Zr}(\text{oxinate})_4$ (average incorporated activity: 34.3 ± 6.0 mBq/cell). Mean \pm SEM of triplicate measures for 3 cell batches.

PET tracking of T cells has been performed with radiolabeled antibodies, antibody fragments, or lipophilic small molecules^{20,21} and by reporter-gene imaging.²² When genetic engineering is not required, e.g., for $\gamma\delta$ -T cells, a clinically applicable alternative to reporter-gene imaging is direct cell labeling with PET radionuclides. Immune cells have long been imaged clinically by single-photon emission computed tomography (SPECT) in this manner, for example, using $[^{111}\text{In}]\text{In}(\text{oxinate})_3$ and $[^{99\text{m}}\text{Tc}]\text{Tc}$ -exametazime.¹⁹ In this regard, the clinically approved 8-hydroxyquinoline (oxine) has been recently shown to be an excellent ionophore for cell labeling with ^{89}Zr ($t_{1/2} = 78.4$ hr, $\beta^+ = 22.3\%$).^{23–25} However, to the best of our knowledge, no study has evaluated its use for tracking $\gamma\delta$ -T cells.

Here we report the first use of $[^{89}\text{Zr}]\text{Zr}(\text{oxinate})_4$ for *in vitro* radiolabeling and *in vivo* tracking of human $\gamma\delta$ -T cells, including the effects of radiolabeling on $\gamma\delta$ -T cell functionality, proliferation, and DNA integrity. We applied this strategy in a xenograft model of breast cancer with an engineered cancer cell line that allows multimodal imaging to track tumor cells. A liposomal aminobisphosphonate was administered to increase T cell trafficking to the tumor.

RESULTS

Radiotracer Labeling Efficiency and Retention in $\gamma\delta$ -T Cells

$[^{89}\text{Zr}]\text{Zr}(\text{oxinate})_4$ was obtained by mixing neutralized $[^{89}\text{Zr}]\text{Zr}(\text{oxalate})_4$ with 8-hydroxyquinoline dissolved in chloroform (Figure 1A). The radiochemical yield was $77.6\% \pm 11.8\%$

(mean \pm SD, $N = 21$), and radiochemical purity established by thin-layer radiochromatography was $>95\%$ (Figure S1). $\gamma\delta$ -T cell labeling efficiency with $[^{89}\text{Zr}]\text{Zr}(\text{oxinate})_4$ ($46.6\% \pm 3.4\%$, $N = 4$) was significantly higher than with $[^{89}\text{Zr}]\text{Zr}(\text{oxalate})_4$ ($6.5\% \pm 1.1\%$, $N = 3$; Figure 1B). To optimize radiolabeling conditions, cells were incubated with $[^{89}\text{Zr}]\text{Zr}(\text{oxinate})_4$ (6–600 mBq/cell) for 10, 20, or 30 min at 4°C , room temperature (RT), or 37°C . We found no significant difference between incubation times and temperatures (Figure S2).

To study long-term tracer retention, radiolabeled $\gamma\delta$ -T cells (25–40 mBq/cell) were cultured at 0.83×10^6 cells/mL. After 24 hr, the percentage of cell-associated ^{89}Zr was $72.9\% \pm 6.8\%$ of the original activity, and $42.4\% \pm 12.6\%$ after 1 week ($N = 3$; Figure 1C).

In Vitro Assays of ^{89}Zr -Radiolabeled $\gamma\delta$ -T Cells

The purity of *in vitro*-expanded $\gamma\delta$ -T cells plateaued 13–15 days post-isolation (Figure S3), at which point they were radiolabeled. Cells labeled with 6–20 mBq/cell proliferated similarly to unlabeled cells ($p \geq 0.05$; Figure 2A), while cells labeled with more than 50 mBq/cell ceased to proliferate *in vitro*, indicating a dose-dependent effect of ^{89}Zr on $\gamma\delta$ -T cell proliferation. A similar dose dependency was observed on $\gamma\delta$ -T cell death (Figure 2B) and DNA damage, evaluated by the formation of γH2AX foci²⁶ 1 hr after labeling (Figures 2C and 2D).

To evaluate the cytotoxic ability of radiolabeled $\gamma\delta$ -T cells, we quantified the survival of MDA-MB-231.hNIS-GFP cancer cell monolayers. $\gamma\delta$ -T cells labeled with up to 600 mBq/cell showed no significant difference in cancer cell killing compared to unlabeled $\gamma\delta$ -T cells (Figure 2E). As a control, adding ^{89}Zr up to 3 Bq/cancer cell in the medium was not toxic to cancer cells in the absence of $\gamma\delta$ -T cells. Even in 30-fold excess, $\gamma\delta$ -T cells showed no toxicity toward cancer cells in the absence of aminobisphosphonate (Figure S4).

In Vivo PET Tracking of ^{89}Zr -Radiolabeled $\gamma\delta$ -T Cells

^{89}Zr -radiolabeled $\gamma\delta$ -T cells were administered intravenously in a mouse xenograft model of breast cancer followed by PET imaging

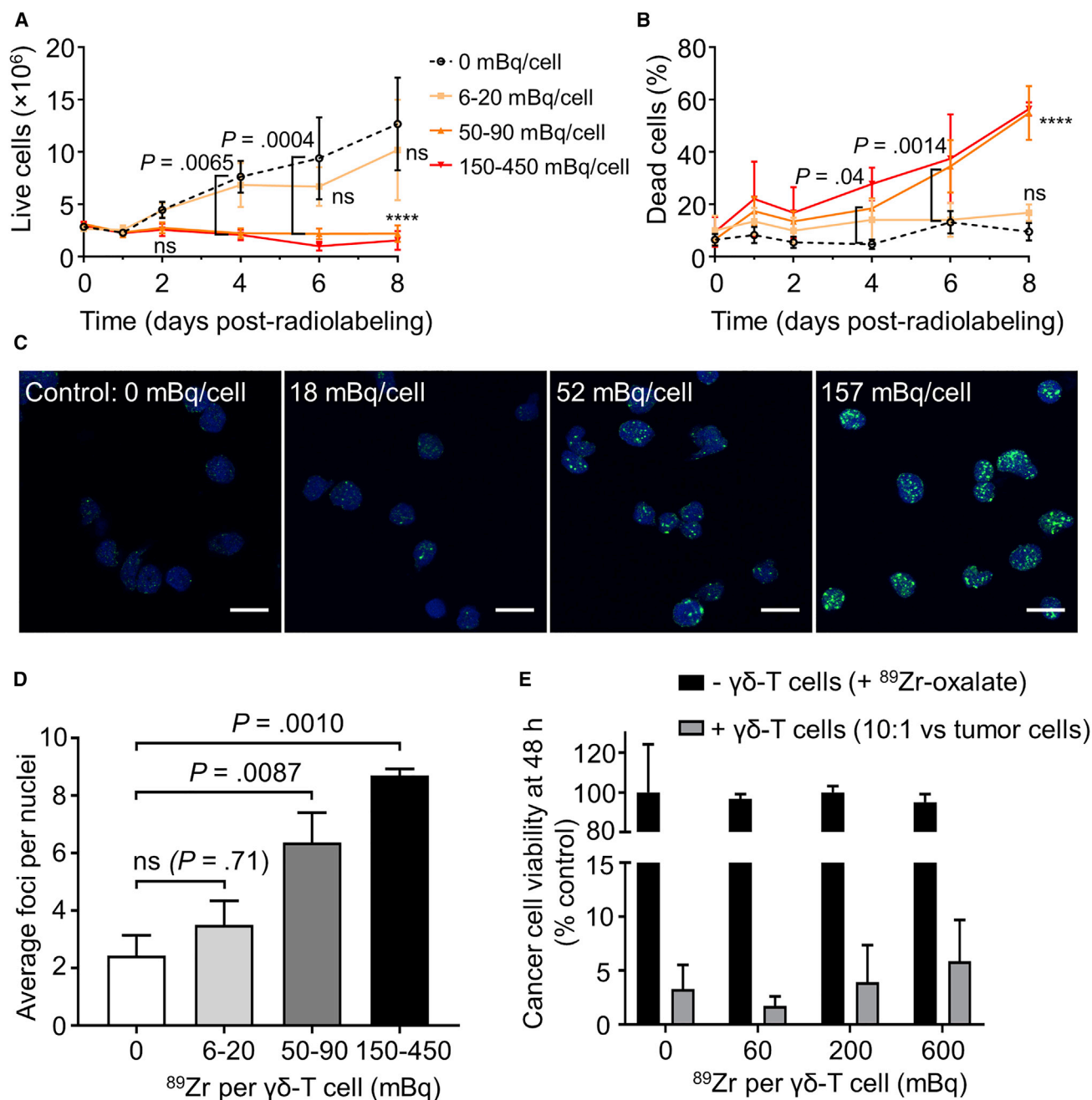
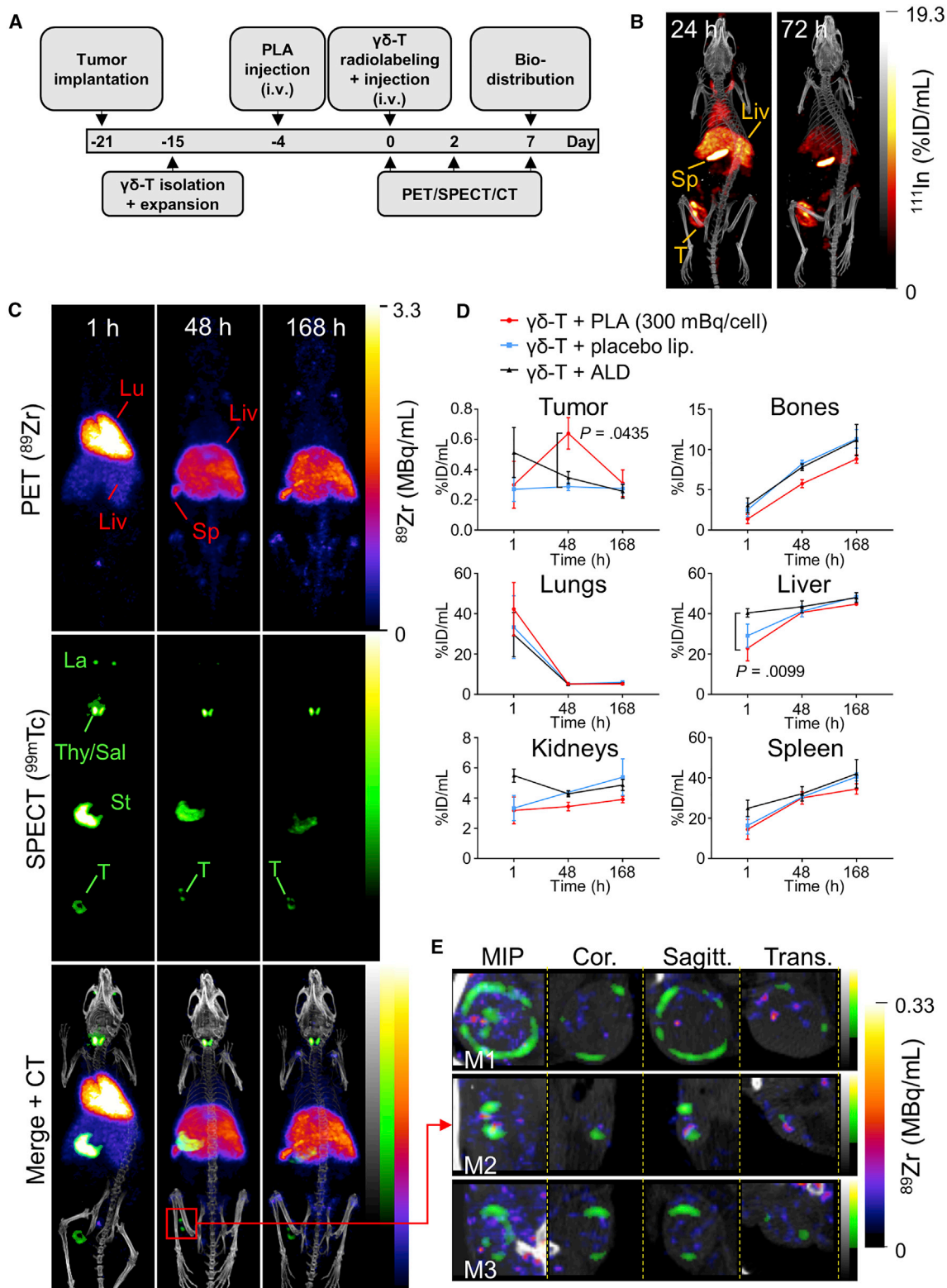


Figure 2. Assays of ^{89}Zr -Radiolabeled $\gamma\delta$ -T Cells

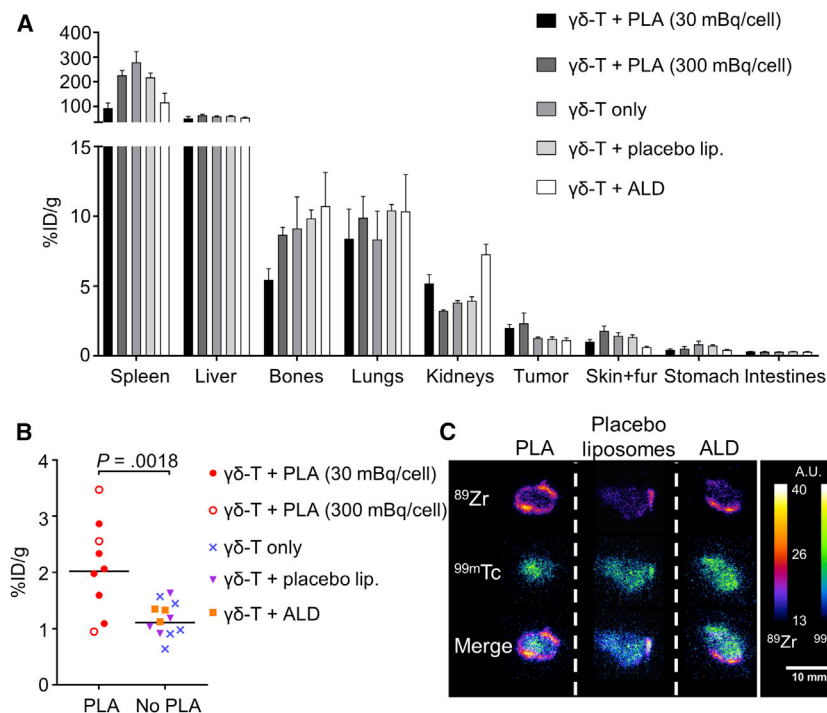
(A and B) *In vitro* growth (A) and mortality (B) of radiolabeled $\gamma\delta$ -T cells. Mean \pm SEM of $N = 4$ independent experiments (except 150–450 mBq group, $N = 2$, not included in statistical analysis). ns: $p > 0.05$; **** $p < 0.0001$ versus unlabeled cells (2-way repeated-measures ANOVA, Dunnett's correction for multiple comparisons). (C) Representative images of γ -H2AX foci (green) and nuclei (blue) in radiolabeled $\gamma\delta$ -T cells (scale bars, 10 μm). (D) Average number of γ -H2AX foci per nuclei after radiolabeling. Mean \pm SEM of $N = 6, 5, 6$, and 3 independent experiments (1-way ANOVA, Dunnett's correction). (E) MDA-MB-231.hNIS-GFP tumor cell viability 48 hr after adding $\gamma\delta$ -T cells or unlabeled ^{89}Zr , expressed as a percentage of control (tumor cells without $\gamma\delta$ -T cells and ^{89}Zr). Mean \pm SEM of $N = 3$ independent experiments (2-way repeated-measures ANOVA, Dunnett's correction).

at 1 hr, 48 hr, and 7 days after injection. We imaged the hNIS-expressing cancer cells by SPECT using $^{99\text{m}}\text{TcO}_4^-$.²⁷ We also evaluated the effect of PLA on $\gamma\delta$ -T cell homing to tumor sites. The study schedule is provided in Figure 3A.

The PLA dosing schedule was established using ^{111}In -labeled PLA, showing significant PLA tumor accumulation within 24–72 hr of administration (Figure 3B; Table S1). The experimental group (PLA treated) received radiolabeled $\gamma\delta$ -T cells + PLA (5 mg/kg alendronate).



(legend on next page)



Control groups (non-PLA treated) received radiolabeled $\gamma\delta$ -T cells with placebo liposomes, non-liposomal alendronate, or saline. An additional control group received $\gamma\delta$ -T cells killed by freeze-thawing to compare bio-distributions of viable and non-viable cells.

SPECT showed uptake of $^{99m}\text{TcO}_4^-$ in tumors and endogenous NIS-expressing organs (thyroid, salivary, and lacrimal glands and stomach; Figure 3C). At 1 hr after intravenous administration of ^{89}Zr -radiolabeled $\gamma\delta$ -T cells, PET revealed high amounts of radioactivity in the lungs in all groups, with signal also observed in the liver and spleen (Figures 3C and 3D). There was significantly higher uptake in the liver in the ALD group versus the PLA group. At tumor sites, the ^{89}Zr signal was close to background (Figure S5). After 48 hr, ^{89}Zr activity increased in the liver, spleen, and bones in all groups and decreased in the lungs. Uptake of ^{89}Zr was observed at the tumor site only in the PLA group (Figure S5), suggesting the presence of radiolabeled $\gamma\delta$ -T cells. Importantly, this was significantly higher in PLA-treated animals compared to control animals treated with non-liposomal alendronate (Figure 3D). Enlarged tumor views showed heterogeneity in tumor tissue, with live tissue, expressing a functional hNIS protein^{18,27} and represented by a donut of ^{99m}Tc signal surrounding a core of non-viable tumor cells

Figure 3. In Vivo Tracking of Radiolabeled $\gamma\delta$ -T Cells

(A) Experiment schedule. (B) Representative SPECT-CT images of MDA-MB-231.hNIS-GFP xenograft NSG mice 24 and 72 hr after ^{111}In -labeled PLA administration. (C) Representative PET, SPECT, and CT (merged) scans of a PLA-treated SCID/beige mouse at 1, 48, and 168 hr post-injection of $\gamma\delta$ -T cells. Liv, liver; Lu, lungs; Sp, spleen; T, tumor. Endogenous murine NIS expression also results in radiotracer uptake, giving rise to the following signals: La, lacrimal glands; St, stomach; and Thy/Sal, thyroid/salivary glands. (D) Time-activity curves from image-based quantification of ^{89}Zr in selected organs. Mean \pm SEM of $N = 3$ –4 animals (repeated-measures MM analysis, Bonferroni correction for multiple comparisons). (E) Enlarged maximum intensity projection (MIP), coronal, sagittal, and transversal tumor views (merged PET- and SPECT-CT) in three PLA-treated mice (M1, M2, and M3), 48 hr after $\gamma\delta$ -T cell injection.

Figure 4. PLA Treatment Increases the Accumulation of $\gamma\delta$ -T Cells in Tumors

(A) *Ex vivo* bio-distribution of radiolabeled $\gamma\delta$ -T cells, 7 days after $\gamma\delta$ -T cell administration. Mean \pm SEM of ^{89}Zr uptake after PLA ($N = 6$ and 3 , respectively), placebo liposomes ($N = 4$), non-liposomal alendronate (ALD; $N = 3$), or vehicle ($N = 5$) treatment. Data are from 3 pooled independent experiments (total $N = 21$). (B) Comparison of ^{89}Zr accumulation in the tumor between PLA ($N = 9$) and non-PLA ($N = 12$) treatments (unpaired *t* test). (C) Artificially colored autoradiographs of tumor sections after PLA, placebo liposomes or non-liposomal alendronate (ALD) treatment. Images are representative of $N = 3$, 4, and 3 animals per group (scale bar, 10 mm).

(Figure 3E). ^{89}Zr signal in tumors was heterogeneous, with some co-localizing with ^{99m}Tc at the edges and foci of ^{89}Zr signal inside the tumor. After 7 days, ^{89}Zr activity remained high in the liver; increased in the spleen, bones, and kidneys; and was indistinguishable from background in tumors. Uptake values are provided in Table S2. Compared to other treatment groups, PET images of killed $\gamma\delta$ -T cells showed a higher accumulation in the liver immediately after injection and increased uptake of ^{89}Zr in the kidneys at later time points (Figure S6).

Ex Vivo Bio-distribution of ^{89}Zr -Radiolabeled $\gamma\delta$ -T Cells

Ex vivo γ -counting 7 days post-administration of radiolabeled cells revealed a high concentration of ^{89}Zr in the spleen ($153.5\% \pm 88.8\%$ injected dose [ID]/g averaged across all groups, $N = 24$) and liver ($58.1\% \pm 10.6\%$ ID/g, $N = 24$) in all groups, followed by lung and bone tissue (Figure 4A). Uptake of ^{89}Zr in tumors from PLA-treated groups ($2.1\% \pm 0.8\%$ ID/g) was significantly higher than in non-PLA groups ($1.2\% \pm 0.3\%$ ID/g; Figure 4B), suggesting higher $\gamma\delta$ -T cell numbers in PLA-treated tumors. Bone uptake of ^{89}Zr in PLA-treated groups ($6.5\% \pm 0.8\%$ ID/g, $N = 9$) was significantly lower than in other groups ($10.0\% \pm 1.1\%$ ID/g, $N = 12$; $p = 0.0238$). Uptake in kidneys was significantly higher with killed $\gamma\delta$ -T cells than in other treatment groups (Table S3). Uptake in other organs showed no major differences between treatment groups.

Tumor section autoradiographs showed a strong signal originating from hNIS-accumulated $^{99m}\text{TcO}_4^-$. Autoradiography was repeated after 4 days to allow for the decay of ^{99m}Tc and the capture ^{89}Zr signal.

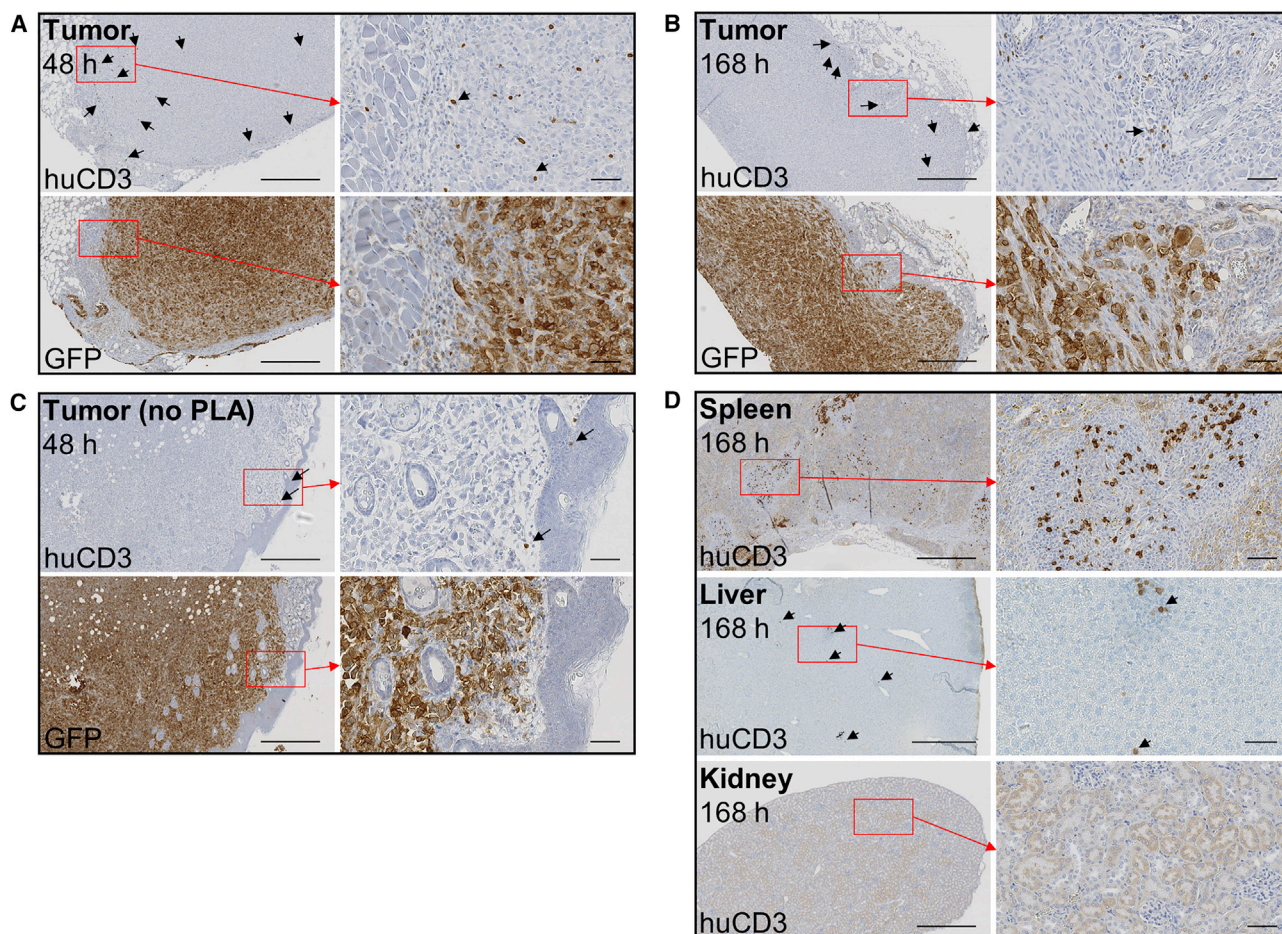


Figure 5. Histology of $\gamma\delta$ -T Cells

(A–C) Tumor sections 48 hr (A and C) or 7 days (B) after the injection of ^{89}Zr -radiolabeled $\gamma\delta$ -T cells into mice treated with PLA (A and B) or without PLA (C), stained for human CD3 ($\gamma\delta$ -T cells) or GFP (tumor cells). Arrows indicate representative CD3⁺ cells. (D) Spleen, liver, and kidney sections 7 days after the administration of ^{89}Zr -radiolabeled $\gamma\delta$ -T cells. Sections are representative of N = 2–3 animals per time point. 6 \times (left) and 30 \times (right) magnification; scale bars, 500 μm (left) and 50 μm (right).

Sections from PLA-treated animals showed increased ^{89}Zr signal compared to non-PLA-treated animals. The ^{89}Zr signal was higher in the tumor periphery, whereas the $^{99\text{m}}\text{Tc}$ signal was uniformly distributed (Figure 4C). $\gamma\delta$ -T cell presence in tumors was demonstrated by immunohistochemistry. Human CD3-positive cells (>95% $\gamma\delta$ -T cell receptor [TCR]⁺ at the time of administration; Figure S3) were visible in tumors 48 hr and 7 days after injection, both in the periphery and deeper regions (Figures 5A–5C; Figure S7). These cells were also visible in the spleen and liver after 7 days, but not in kidney sections (Figure 5D) or in control tissues of mice not administered $\gamma\delta$ -T cells (Figure S8).

DISCUSSION

[^{89}Zr]Zr(oxinate)₄ synthesis has been reported previously by our group²³ and others.^{24,25} The temperature-independent labeling efficiency of $\gamma\delta$ -T cells with [^{89}Zr]Zr(oxinate)₄ suggests this is a passive process, in line with results from Sato et al.²⁴ Sufficient radiotracer retention within cells is important to ensure that the imaging signal

reflects labeled cells rather than free radiotracer bio-distribution. We observed an efflux of approximately half of the incorporated ^{89}Zr over 1 week *in vitro*, which we believe does not interfere with *in vivo* imaging within this time frame. Uptake of ^{89}Zr in the bone can be used to estimate the amount of tracer that leaked from the cells.^{25,28} Retention of [^{89}Zr]Zr(oxinate)₄ is dependent on cell type, and our results are comparable to those observed with dendritic, bone marrow, and chimeric antigen receptor (CAR)-T cells.^{23–25} Comparable levels of tracer efflux have been observed from lymphocytes labeled with [^{111}In]In(oxinate)₃,^{29,30} the current gold standard for cell tracking by nuclear imaging.

A radiotracer for cell tracking must not significantly alter the phenotype, survival, proliferation capacity, and functionality of labeled cells. We demonstrated that the effects of [^{89}Zr]Zr(oxinate)₄ on $\gamma\delta$ -T cell survival, proliferation capacity, and DNA damage were kept minimal for doses up to 20 mBq/cell but were significant at doses ≥ 50 mBq/cell. The cytotoxicity of radiolabeled $\gamma\delta$ -T cells

against the same tumor cells used for *in vivo* experiments was not affected by amounts of [^{89}Zr]Zr(oxinate) $_4$ of up to 600 mBq/cell, at least within 48 hr of radiolabeling. Cancer cell death was due to the combination of bisphosphonate treatment and $\gamma\delta$ -T cells and not to the presence of ^{89}Zr . Preserved cytotoxicity after radiolabeling, also recently observed in CAR-T cells by Weist et al.,²⁵ is encouraging for the use of [^{89}Zr]Zr(oxinate) $_4$ as a T cell-tracking agent. However, the therapeutic efficacy of $\gamma\delta$ -T cells presumably also relies on their *in vivo* proliferation ability; hence, we suggest that radiolabeling $\gamma\delta$ -T cells with [^{89}Zr]Zr(oxinate) $_4$ should ideally not exceed 20 mBq/cell. This could lead to sensitivity issues on conventional PET scanners. Indeed, our experiments show that *ex vivo* gamma-counting tumors could reveal amounts of ^{89}Zr indistinguishable from background in our PET imaging system at day 7. Assuming that a human cell-tracking study would require 37 MBq ^{89}Zr ³¹ and 10^9 $\gamma\delta$ -T cells,¹⁴ this would equate to an average of 37 mBq/cell, which we have shown not to be excessively damaging to $\gamma\delta$ -T cells. Upcoming developments in PET technology, such as total-body PET,³² should reduce the required ^{89}Zr activity per cell (by a factor of 40) and overcome these sensitivity issues.

For *in vivo* studies, a xenograft model of human breast cancer in immunocompromised mice^{12,33} was chosen, as mice do not possess a subset of T cells functionally equivalent to human V γ 9V δ 2 T cells.³⁴ We tracked $\gamma\delta$ -T cells radiolabeled with [^{89}Zr]Zr(oxinate) $_4$ (30–300 mBq/cell) by PET 1 hr, 48 hr, and 7 days after intravenous injection. We simultaneously used $^{99\text{m}}\text{TcO}_4^-$ to visualize hNIS-expressing tumors by SPECT. The *in vivo* distribution of ^{89}Zr -labeled $\gamma\delta$ -T cells over time was similar to that observed in studies of adoptively transferred $\gamma\delta$ -T^{35,36} and other T cells.^{25,37,38} ^{89}Zr uptake was significantly increased in PLA-treated tumors, suggesting that PLA increases homing of these cells to the tumor site. Accumulation of $\gamma\delta$ -T cells at the tumor site 48 hr after administration was also observed by others.³⁵ Uptake values for the spleen and tumor determined by image-based quantification are lower than those determined by *ex vivo* bio-distribution. This can be explained by the small size of this organ and significant partial volume effect (spleen) and the liquid or necrotic tumor core that leaked upon dissection.

For instrument sensitivity reasons, some imaging studies were performed with higher doses of ^{89}Zr than recommended above. However, the distinctly different distribution pattern observed with killed $\gamma\delta$ -T cells suggests that radiolabeling with up to 300 mBq/cell, which preserved cytotoxic functionality *in vitro* over 48 hr, did not impair $\gamma\delta$ -T cell trafficking and allowed us to track live cells. Furthermore, previous studies have shown that [^{89}Zr]Zr(oxalate) $_4$,^{28,39} [^{89}Zr]Zr(oxinate) $_4$, and lysates from [^{89}Zr]Zr(oxinate) $_4$ -labeled cells²³ have distinct distribution patterns from intact cells labeled with [^{89}Zr]Zr(oxinate) $_4$. Cell concentrations during labeling and *in vitro* assays were in the range of $1\text{--}5 \times 10^6/\text{mL}$. In comparison, using *in vitro* ^{89}Zr retention values, cell concentrations extrapolated from PET-computed tomography (CT) images in the organs showing the strongest ^{89}Zr signal (spleen, liver, and lungs) would be in the range of $0.5\text{--}5 \times 10^6$ cells/mL. We therefore expect the DNA damage sus-

tained by $\gamma\delta$ -T cells, due to both self-irradiation and crossfire, after *in vivo* administration to be comparable to that observed *in vitro*. Considering the strong affinity of the $^{89}\text{Zr}^{4+}$ ion for bone,²⁸ the relatively low bone accumulation of ^{89}Zr indicates limited efflux of weakly chelated ^{89}Zr , and it suggests that ^{89}Zr is mostly retained by $\gamma\delta$ -T cells after injection. The lower accumulation of ^{89}Zr in the bones of PLA-treated animals compared to other groups also suggests reduced efflux of ^{89}Zr from $\gamma\delta$ -T cells after PLA treatment.

Histology confirmed the presence of $\gamma\delta$ -T cells in the tumors, spleen, and liver, using the CD3 marker.⁴⁰ Immunohistochemistry and autoradiography suggest that $\gamma\delta$ -T cells accumulated mostly at the periphery of the tumor. The small number of cells observed by immunohistochemistry precludes statistical comparison. Furthermore, these techniques can only image the solid portion of the tumor. PET imaging not only allowed visualization of the whole, intact tumors but additionally revealed heterogeneous distributions of ^{89}Zr in tumors, which would be challenging to observe by histology. Combined with the non-invasive nature of PET imaging, this further highlights the value of using PET tracers such as [^{89}Zr]Zr(oxinate) $_4$ for cell tracking. The high uptake of ^{89}Zr in the liver and spleen was mirrored by the large numbers of human CD3 $^+$ cells observed in these tissues, consistent with the bio-distribution of radiolabeled $\gamma\delta$ -T cells. In contrast, the apparent absence of CD3 $^+$ cells in the kidneys, despite higher ^{89}Zr uptake than in the tumor, and the fact that the kidney uptake of ^{89}Zr was significantly higher in animals administered killed $\gamma\delta$ -T cells than in other groups both suggest that the radioactivity detected in the kidneys corresponds to ^{89}Zr progressively released from $\gamma\delta$ -T cells in other organs. A limitation of directly labeling cells is that the radionuclide can leak out over time and be taken up by adjacent tissue. Although immunohistochemistry demonstrates the presence of the administered $\gamma\delta$ -T cells in the tumors, this technique cannot determine whether the ^{89}Zr signal originates from the $\gamma\delta$ -T cells or from *in situ*-labeled bystander cells.

A critical aspect of this type of cellular immunotherapy is that the therapeutic cells must be activated at the target site and reach the tumor in sufficient numbers. $\gamma\delta$ -T cell toxicity toward cancer cells is greatly amplified by bisphosphonates, suggesting a role for $\gamma\delta$ -T cells in the anti-cancer properties of bisphosphonates.⁴¹ Here we sought to increase phosphoantigen expression in tumors by administering PLA, which delivers alendronate to the tumors in an untargeted fashion by virtue of the enhanced permeability and retention (EPR) effect.⁴² Liposomal alendronate proved safer than other bisphosphonates and effective in potentiating $\gamma\delta$ -T cell therapy.^{12,43} We have previously shown that the tumor-to-background uptake ratio of PLA increases over time and is significant after 3 days.⁴⁴ Here we observed that PLA administered 4 days in advance significantly increased the amount of ^{89}Zr reaching the tumor within 48 hr of radiolabeled $\gamma\delta$ -T cell administration. Our results suggest that $\gamma\delta$ -T cells home to the tumor within 2 days and remain there for at least 5 days. This was not observed in any other treatment group, demonstrating the importance of encapsulating the aminobisphosphonate in a tumor-targeting vehicle.

Clinical imaging studies of therapeutic T cells with [^{111}In]In(oxinate)₃ have been performed by radiolabeling only a fraction of the total administered T cells,^{45–47} although evidence exists that distributing the total activity over a larger number of cells better preserves their proliferative abilities.⁴⁸ Our results suggest that radiolabeling the entire batch of $\gamma\delta$ -T cells with [^{89}Zr]Zr(oxinate)₄ might be the preferable option to avoid imaging excessively damaged cells. In two notable studies, γ -scintigraphy revealed T cell uptake in tumors using only 1–3 mBq ^{111}In per cell.^{46,49} Considering the increased sensitivity of PET over SPECT and expected improvements in PET technology, clinical imaging of T cell therapies using [^{89}Zr]Zr(oxinate)₄ is a credible prospect.

Conclusions

This study demonstrates the suitability of [^{89}Zr]Zr(oxinate)₄ as a PET tracer to track $\gamma\delta$ -T cells *in vivo*, while previous work has shown the therapeutic efficacy of $\gamma\delta$ -T cells in combination with PLA.^{12,43} These objectives achieved, [^{89}Zr]Zr(oxinate)₄ can now be applied to answer fundamental questions in the preclinical and clinical development of $\gamma\delta$ -T cell therapies, e.g., whether the accumulation of $\gamma\delta$ -T cells at the tumor site or their distribution within the tumor correlates with therapeutic efficacy. Due to numerous molecular and cellular differences, the distribution of human $\gamma\delta$ -T cells in an immunocompromised mouse model cannot fully predict their behavior in a human host. However, the results of this proof-of-principle study can be used to design a clinical trial that will answer the question of the distribution of $\gamma\delta$ -T cells in humans after adoptive transfer.

Our results have implications for clinical translation, and they suggest using liposomal aminobisphosphonates as adjuncts to $\gamma\delta$ -T cell therapy. In the context of clinical protocols involving repeated infusions of $\gamma\delta$ -T cells,¹⁵ one can envisage the use of ^{89}Zr -labeled cells for the first infusion, followed by PET imaging 24–72 hr later. The number of cells trafficking to the tumor sites would then be used to decide whether to pursue with additional treatment cycles. Cell radiolabeling with [^{89}Zr]Zr(oxinate)₄ is clinically translatable without significant methodological modifications, and the high similarity of [^{89}Zr]Zr(oxinate)₄ to the well-established [^{111}In]In(oxinate)₃ should facilitate regulatory approval. Our results support that T cell labeling with [^{89}Zr]Zr(oxinate)₄ is a realistic option for human studies and will benefit the development of cellular immunotherapy.

MATERIALS AND METHODS

Experiment Approval

Animals experiments were approved by the UK Home Office under The Animals (Scientific Procedures) Act (1986), PPL reference 7008879 (Protocol 6), with local approval from King's College London Research Ethics Committee (KCL-REC). Experiments using human T cells received approval from KCL-REC (Study Reference HR-16/17-3746). All donors provided written, informed consent.

Reagents, Animals, and Cells

Unless otherwise indicated, reagents were purchased from Sigma-Aldrich and Merck. Female SCID/beige (CB17.Cg-Prkdc^{scid}Lyst^{bgJ}/CrI)

and Nod scid gamma (NSG) (NOD.Cg-Prkdc^{scid} Il2rg^{tm1Wjl}/SzJ) mice (18–25 g, 10–20 weeks old) were obtained from Charles River (UK). $\gamma\delta$ -T cells were obtained as described previously,¹² using zoledronate (Novartis) and interleukin-2 (IL-2) (Novartis). Full details are provided in the [Supplemental Materials and Methods](#). Population purity was assessed by flow cytometry (BD FACSCalibur), using pan- $\gamma\delta$ TCR (IMMU510, Beckman Coulter B49175) and anti-CD3 (OKT3, BioLegend 317307) monoclonal antibodies. Data were analyzed using Flowing version (v.)2.5.1 (<http://flowingsoftware.btk.fi>). Only batches with $\geq 80\%$ $\gamma\delta$ -positive CD3⁺ cells were used for further experiments ($\geq 95\%$ for *in vivo* experiments). MDA-MB-231.hNIS-GFP cells²⁷ were grown in DMEM supplemented with 10% fetal bovine serum (FBS), penicillin, streptomycin, and L-glutamine (2 mM), and they were tested for mycoplasma contamination (e-Myco PCR detection kit, Bulldog Bio).

PET Tracer Synthesis

[^{89}Zr]Zr(oxinate)₄ was synthesized as previously described.²³ Full details are provided in the [Supplemental Materials and Methods](#).

Cell Labeling

$\gamma\delta$ -T cells expanded *in vitro*¹² were washed with PBS (Ca²⁺/Mg²⁺ free) and re-suspended at $5 \times 10^6/\text{mL}$ in PBS at RT. [^{89}Zr]Zr(oxinate)₄ (6–600 mBq/cell) in aqueous DMSO was added to the cell suspension, keeping DMSO concentrations $\leq 0.7\%$. Neutralized [^{89}Zr]Zr(oxalate)₄ with an equivalent amount of DMSO was used as a control. After 10–30 min of incubation, cells were pelleted and the supernatants kept aside. The cells were washed with PBS, centrifuged, and the washings combined with the previous supernatants. The cells were suspended in growth medium or PBS for further experiments. Viability was assessed using the trypan blue dye exclusion method. Radioactivity in re-suspended cells and combined supernatants was measured in a gamma-counter. Cell-labeling efficiency (LE[%]) was calculated as follows.

$$LE(\%) = \frac{\text{activity of cell fraction}}{\text{activity of cell fraction} + \text{activity of combined supernatants}}$$

For radiotracer retention and cell proliferation studies, radiolabeled (or vehicle-treated) $\gamma\delta$ -T cells were cultured as described above, and they were analyzed at various time points for viability (using trypan blue), determination of cell-associated radioactivity (by γ -counting), and cell death (by flow cytometry using propidium iodide [PI]; Thermo Scientific). Further details are provided in the [Supplemental Materials and Methods](#).

Cancer Cell-Killing Assay

MDA-MB-231.hNIS-GFP cells seeded in a 96-well plate at 10^4 cells/well and incubated overnight were treated with 3 μM zoledronate or vehicle for 24 hr. The cells were washed and the medium was replaced with $\gamma\delta$ -T cells in growth medium. As a control for radiolabeled $\gamma\delta$ -T cells, an equal amount of ^{89}Zr in medium was added to some wells. After 48 hr, $\gamma\delta$ -T cells were removed by washing with PBS, and cancer cell viability was evaluated using the alamarBlue assay (Thermo

Scientific), reading plates in a GloMax (Promega) reader (530 nm excitation and 590 nm emission filters).

Determination of DNA Double-Strand Breaks

Radiolabeled $\gamma\delta$ -T cells in medium were seeded onto poly-L-lysine-coated coverslips and incubated for 1 hr. After centrifugation and gentle rinsing with PBS, the cells were fixed and permeabilized with 3.7% formalin, 0.5% Triton X-100, and 0.5% IGEPAL CA-630 in PBS, then blocked with 2% BSA and 1% goat serum. γ H2AX foci were detected with an anti- γ H2AX (Ser139) mouse monoclonal antibody (mAb) (1:1,600; JBW301, Merck 05-636) and goat anti-mouse AF488-immunoglobulin G (IgG) (1:500; Jackson ImmunoResearch Laboratories 115-545-062). Nuclei were detected with Hoechst 33342. Images were acquired on a TCS SP5 II confocal microscope (Leica) with a 100 \times /1.40 HCX PL Apochromat objective (Leica) and Leica Application Suite Advanced Fluorescence (LAS-AF) control software. Ten sections (0.4- μ m thickness) were imaged. At least 30 nuclei/slide were imaged (2 slides/treatment). Maximal intensity projections of z stacks were made using ImageJ v.1.51p (<https://imagej.nih.gov/ij/>). Nuclei and γ H2AX foci were counted using CellProfiler v.2.2.0 (<http://cellprofiler.org>), calculating average numbers of γ H2AX foci per nucleus in each image. Full details are provided in the [Supplemental Materials and Methods](#).

Animals, Tumor Model, and Tumor Sensitization with Liposomal Alendronate

Approximately 1.5×10^6 MDA-MB-231.hNIS-GFP cells were injected subcutaneously in the mammary fat pad between the fourth and fifth nipples in the left flank; tumors were grown over 3 weeks. Animals were randomly assigned to experimental groups, and investigators were not blinded to cohort allocation when assessing outcomes. Cohort sizes were chosen based on prior experience,^{44,50} in compliance with local regulations concerning animal experiments. Liposomal formulations were prepared at Shaare Zedek MC as previously described.¹³ Alendronate-loaded liposomes (PLA) contained 1.5–5.4 mg/mL alendronate and 36–40 μ mol/mL phospholipids. Placebo liposomes contained 20–50 μ mol/mL phospholipids. PLA was co-injected with placebo liposomes for a total dose of 5 mg/kg alendronate and 4 μ mol phospholipids per mouse in PLA-treated animals. Placebo-treated animals received empty liposomes corresponding to 4 μ mol phospholipids per mouse. Another control group received 5 mg/kg alendronate (ALD). Formulations were injected intravenously (i.v.) 4 days before the administration of radiolabeled $\gamma\delta$ -T cells.

In Vivo PET and SPECT Imaging of $\gamma\delta$ -T Cells, Tumors, and PLA

⁸⁹Zr-radiolabeled $\gamma\delta$ -T cells (10^7 cells/animal in 100 μ L, 0.3–3 MBq ⁸⁹Zr, single $\gamma\delta$ -T donor per experiment) were injected i.v. at t = 0 hr and imaged by PET/CT within 30 min. PET/CT imaging was performed for 30–240 min (as indicated) on a nanoScan PET-CT scanner (Mediso). For tumor imaging, 100 μ L ^{99m}TcO₄[−] (15–25 MBq) in saline was injected i.v., and SPECT-CT was performed 40 min thereafter in a NanoSPECT/CT scanner (Mediso; 1-mm collimators, 30-min scan). PET-CT and SPECT-CT were repeated at t = 48 and 168 hr. For PLA imaging by SPECT-CT, PLA was radiolabeled with

[¹¹¹In]In(oxinate)₃ and administered i.v. (7 MBq ¹¹¹In/mouse) to NSG mice. PET- and SPECT-CT datasets were reconstructed using a Monte Carlo-based full-3D iterative algorithm (Tera-Tomo, Mediso). Images were co-registered and analyzed using VivoQuant v.2.50 (Invivo). Regions of interest (ROIs) were delineated for PET activity quantification in specific organs. Uptake in each ROI was expressed as a percentage of injected dose per volume (% ID/mL).

Ex Vivo Bio-distribution Studies

Mice from imaging studies were used for bio-distribution studies on day 2 or 7. After culling, organs were dissected, weighed, and γ -counted together with standards prepared from a sample of injected material. The percentage of injected dose per gram (% ID/g) of tissue was calculated. Organs were cryopreserved in optimal cutting temperature (OCT) compound (VWR) for autoradiography and/or formalin fixed and paraffin embedded (FFPE) for histologic analysis.

Autoradiography

Cryopreserved tissues were cut (50 μ m), mounted on poly-L-lysine-coated slides (VWR), fixed in 4% paraformaldehyde (PFA), mounted in Mowiol, and exposed to a storage phosphor screen for 20 min at 3 hr post-dissection to obtain the ^{99m}Tc signal, then for 48 hr at 4 days post-dissection to obtain the ⁸⁹Zr signal. The storage phosphor screen was read using a Cyclone Plus imager (PerkinElmer), and images were processed with ImageJ.

Immunohistochemistry

Briefly, FFPE organ blocks were sliced and stained using a Discovery XT system (Ventana Medical Systems) using the DAB Map detection kit (Ventana 760-124). For pre-treatment, CC1 (Ventana 950-124) was used. Sections were stained with anti-GFP (1/1,000; Abcam ab290, UK) or anti-CD3 (LN10, Leica CD3-565-L-CE) primary antibodies, followed by biotinylated anti-rabbit or anti-mouse IgG (1/200; Dako) secondary antibodies, as appropriate. Full details are provided in the [Supplemental Materials and Methods](#).

Statistics

Independent experiments were performed on different days with $\gamma\delta$ -T cell batches from different donors. Data were plotted using Prism v.7.01 (GraphPad). Differences between 2 groups were evaluated by Student's two-tailed t test. To account for repeated measurements in a same animal or cell batch and multiple treatments tested on a same cell batch, analysis was performed using 2-way repeated-measures ANOVA in GraphPad Prism or a repeated-measures Mixed Model (MM)⁵¹ in InVivoStat v.3.7 (<http://invivostat.co.uk/>), as indicated. Dunnett's post hoc test was applied for comparisons back to a control group, or Bonferroni correction for multiple pairwise comparisons, unless otherwise specified. Exact significance values are reported in each figure.

SUPPLEMENTAL INFORMATION

Supplemental Information includes eight figures, three tables, and Supplemental Materials and Methods and can be found with this article online at <https://doi.org/10.1016/j.ymthe.2018.10.006>.

AUTHOR CONTRIBUTIONS

Conceptualization, F.M., L.L., G.O.F., and R.T.M.d.R.; Methodology, F.M., L.L., A.G., G.O.F., and R.T.M.d.R.; Investigation, F.M., L.L., A.V., B.D., A.C.P.-P., and R.T.M.d.R.; Writing – Original Draft, F.M.; Writing – Review and Editing, F.M., L.L., A.G., J.M., P.J.B., G.O.F., and R.T.M.d.R.; Funding Acquisition, G.O.F., R.T.M.d.R., P.J.B., and J.M.; Resources, F.M., L.L., A.G., H.S., and R.T.M.d.R.; Supervision, R.T.M.d.R., G.O.F., and P.J.B.

CONFLICTS OF INTEREST

J.M. is chief scientific officer of Leucid Bio, a company dedicated to the commercial development of CAR-T cells for solid tumors. The authors declare no other potential conflicts of interest.

ACKNOWLEDGMENTS

The authors thank J. Bartnicka, Dr. J. Bordoloi, A. Dzhatdova, P. Gawne, I. Hungnes, M. Iafrate, and G. Keeling for technical assistance. This work was supported by a Cancer Research UK (CRUK) Multidisciplinary Project Award (grant C48390/A21153), the KCL/UCL Comprehensive Cancer Imaging Centre funded by CRUK and EPSRC in association with the MRC and DoH (England), the Wellcome EPSRC Centre for Medical Engineering at KCL (grant WT 203148/Z/16/Z), the Medical Research Council Confidence in Concepts scheme, the Experimental Cancer Medicine Centre at KCL, the KHP/KCL CRUK Cancer Centre and the National Institute for Health Research (NIHR) Biomedical Research Centre based at Guy's and St Thomas' NHS Foundation Trust and KCL (grant IS-BRC-1215-20006). The views expressed are those of the authors and not necessarily those of the NHS, the NIHR, or the Department of Health.

REFERENCES

- Turtle, C.J., Hay, K.A., Hanafi, L.-A., Li, D., Cherian, S., Chen, X., Wood, B., Lozanski, A., Byrd, J.C., Heimfeld, S., et al. (2017). Durable molecular remissions in chronic lymphocytic leukemia treated with CD19-specific chimeric antigen receptor-modified T cells after failure of ibrutinib. *J. Clin. Oncol.* 35, 3010–3020.
- Chandran, S.S., Somerville, R.P.T., Yang, J.C., Sherry, R.M., Klebanoff, C.A., Goff, S.L., Wunderlich, J.R., Danforth, D.N., Zlott, D., Paria, B.C., et al. (2017). Treatment of metastatic uveal melanoma with adoptive transfer of tumour-infiltrating lymphocytes: a single-centre, two-stage, single-arm, phase 2 study. *Lancet Oncol.* 18, 792–802.
- Rosenberg, S.A., and Restifo, N.P. (2015). Adoptive cell transfer as personalized immunotherapy for human cancer. *Science* 348, 62–68.
- Gentles, A.J., Newman, A.M., Liu, C.L., Bratman, S.V., Feng, W., Kim, D., Nair, V.S., Xu, Y., Khuong, A., Hoang, C.D., et al. (2015). The prognostic landscape of genes and infiltrating immune cells across human cancers. *Nat. Med.* 21, 938–945.
- Tyler, C.J., Doherty, D.G., Moser, B., and Eberl, M. (2015). Human V γ 9/V δ 2 T cells: Innate adaptors of the immune system. *Cell. Immunol.* 296, 10–21.
- Vantourout, P., and Hayday, A. (2013). Six-of-the-best: unique contributions of $\gamma\delta$ T cells to immunology. *Nat. Rev. Immunol.* 13, 88–100.
- Bouet-Toussaint, F., Cabillat, F., Toutirais, O., Le Gallo, M., Thomas de la Pintière, C., Daniel, P., Genet, N., Meunier, B., Dupont-Bierre, E., Boudjema, K., and Catros, V. (2008). V γ 9V δ 2 T cell-mediated recognition of human solid tumors. Potential for immunotherapy of hepatocellular and colorectal carcinomas. *Cancer Immunol. Immunother.* 57, 531–539.
- Gu, S., Sachleben, J.R., Boughter, C.T., Nawrocka, W.I., Borowska, M.T., Tarrasch, J.T., Skiniotis, G., Roux, B., and Adams, E.J. (2017). Phosphoantigen-induced conformational change of butyrophilin 3A1 (BTN3A1) and its implication on V γ 9V δ 2 T cell activation. *Proc. Natl. Acad. Sci. USA* 114, E7311–E7320.
- Vavassori, S., Kumar, A., Wan, G.S., Ramanjaneyulu, G.S., Cavallari, M., El Daker, S., Beddoe, T., Theodossis, A., Williams, N.K., Gostick, E., et al. (2013). Butyrophilin 3A1 binds phosphorylated antigens and stimulates human $\gamma\delta$ T cells. *Nat. Immunol.* 14, 908–916.
- De Rosa, G., Misso, G., Salzano, G., and Caraglia, M. (2013). Bisphosphonates and cancer: what opportunities from nanotechnology? *J. Drug Deliv.* 2013, 637976.
- Kunzmann, V., Bauer, E., Feurle, J., Weissinger, F., Tony, H.P., and Wilhelm, M. (2000). Stimulation of gammadelta T cells by aminobisphosphonates and induction of antiplasma cell activity in multiple myeloma. *Blood* 96, 384–392.
- Parente-Pereira, A.C., Shmeeda, H., Whilding, L.M., Zambirinis, C.P., Foster, J., van der Stegen, S.J.C., Beatson, R., Zabinski, T., Brewig, N., Sosabowski, J.K., et al. (2014). Adoptive immunotherapy of epithelial ovarian cancer with V γ 9V δ 2 T cells, potentiated by liposomal alendronic acid. *J. Immunol.* 193, 5557–5566.
- Shmeeda, H., Amitay, Y., Gorin, J., Tzemach, D., Mak, L., Stern, S.T., Barenholz, Y., and Gabizon, A. (2016). Coencapsulation of alendronate and doxorubicin in pegylated liposomes: a novel formulation for chemimmunotherapy of cancer. *J. Drug Target.* 24, 878–889.
- Kobayashi, H., and Tanaka, Y. (2015). $\gamma\delta$ T cell immunotherapy—A review. *Pharmaceuticals (Basel)* 8, 40–61.
- Fisher, J.P., Heuvelink, J., Yan, M., Gustafsson, K., and Anderson, J. (2014). $\gamma\delta$ T cells for cancer immunotherapy: A systematic review of clinical trials. *Oncol Immunology* 3, e27572.
- James, M.L., and Gambhir, S.S. (2012). A molecular imaging primer: modalities, imaging agents, and applications. *Physiol. Rev.* 92, 897–965.
- Ponomarev, V. (2017). Advancing immune and cell-based therapies through imaging. *Mol. Imaging Biol.* 19, 379–384.
- Volpe, A., Kurtys, E., and Fruhwirth, G.O. (2018). Cousins at work: How combining medical with optical imaging enhances in vivo cell tracking. *Int. J. Biochem. Cell Biol.* 102, 40–50.
- Kircher, M.F., Gambhir, S.S., and Grimm, J. (2011). Noninvasive cell-tracking methods. *Nat. Rev. Clin. Oncol.* 8, 677–688.
- Tavaré, R., McCracken, M.N., Zettlitz, K.A., Knowles, S.M., Salazar, F.B., Olafsen, T., Witte, O.N., and Wu, A.M. (2014). Engineered antibody fragments for immuno-PET imaging of endogenous CD8+ T cells in vivo. *Proc. Natl. Acad. Sci. USA* 111, 1108–1113.
- Mall, S., Yusufi, N., Wagner, R., Klar, R., Bianchi, H., Steiger, K., Straub, M., Audehm, S., Laitinen, I., Aichler, M., et al. (2016). Immuno-PET imaging of engineered human T cells in tumors. *Cancer Res.* 76, 4113–4123.
- Jurgielewicz, P., Harmsen, S., Wei, E., Bachmann, M.H., Ting, R., and Aras, O. (2017). New imaging probes to track cell fate: reporter genes in stem cell research. *Cell. Mol. Life Sci.* 74, 4455–4469.
- Charoenphun, P., Meszaros, L.K., Chuamsaamarkkee, K., Sharif-Paghaleh, E., Ballinger, J.R., Ferris, T.J., Went, M.J., Mullen, G.E., and Blower, P.J. (2015). [^{89}Zr]oxinate₄ for long-term in vivo cell tracking by positron emission tomography. *Eur. J. Nucl. Med. Mol. Imaging* 42, 278–287.
- Sato, N., Wu, H., Asiedu, K.O., Szajek, L.P., Griffiths, G.L., and Choyke, P.L. (2015). ^{89}Zr -oxine complex PET cell imaging in monitoring cell-based therapies. *Radiology* 275, 490–500.
- Weist, M.R., Starr, R., Aguilar, B., Chea, J., Miles, J.K., Poku, E., Gerdt, E., Yang, X., Priceman, S.J., Forman, S.J., et al. (2018). PET of adoptively transferred chimeric antigen receptor T cells with ^{89}Zr -oxine. *J. Nucl. Med.* 59, 1531–1537.
- Bonner, W.M., Redon, C.E., Dickey, J.S., Nakamura, A.J., Sedelnikova, O.A., Solier, S., and Pommier, Y. (2008). GammaH2AX and cancer. *Nat. Rev. Cancer* 8, 957–967.
- Volpe, A., Man, F., Lim, L., Khoshnevisan, A., Blower, J., Blower, P.J., and Fruhwirth, G.O. (2018). Radionuclide-fluorescence Reporter Gene Imaging to Track Tumor Progression in Rodent Tumor Models. *J. Vis. Exp.* (133).
- Abou, D.S., Ku, T., and Smith-Jones, P.M. (2011). In vivo biodistribution and accumulation of ^{89}Zr in mice. *Nucl. Med. Biol.* 38, 675–681.

29. ten Berge, R.J., Natarajan, A.T., Hardeman, M.R., van Royen, E.A., and Schellekens, P.T. (1983). Labeling with indium-111 has detrimental effects on human lymphocytes: concise communication. *J. Nucl. Med.* 24, 615–620.
30. Kuyama, J., McCormack, A., George, A.J., Heelan, B.T., Osman, S., Batchelor, J.R., and Peters, A.M. (1997). Indium-111 labelled lymphocytes: isotope distribution and cell division. *Eur. J. Nucl. Med.* 24, 488–496.
31. Jauw, Y.W.S., Menke-van der Houven van Oordt, C.W., Hoekstra, O.S., Hendrikse, N.H., Vugts, D.J., Zijlstra, J.M., Huisman, M.C., and van Dongen, G.A. (2016). Immuno-Positron Emission Tomography with Zirconium-89-Labeled Monoclonal Antibodies in Oncology: What Can We Learn from Initial Clinical Trials? *Front. Pharmacol.* 7, 131.
32. Zhang, X., Zhou, J., Cherry, S.R., Badawi, R.D., and Qi, J. (2017). Quantitative image reconstruction for total-body PET imaging using the 2-meter long EXPLORER scanner. *Phys. Med. Biol.* 62, 2465–2485.
33. Hodgins, N.O., Al-Jamal, W.T., Wang, J.T.-W., Klippstein, R., Costa, P.M., Sosabowski, J.K., Marshall, J.F., Maher, J., and Al-Jamal, K.T. (2017). Investigating in vitro and in vivo $\alpha v \beta 6$ integrin receptor-targeting liposomal alendronate for combinatory $\gamma \delta$ T cell immunotherapy. *J. Control. Release* 256, 141–152.
34. Pang, D.J., Neves, J.F., Sumaria, N., and Pennington, D.J. (2012). Understanding the complexity of $\gamma \delta$ T-cell subsets in mouse and human. *Immunology* 136, 283–290.
35. Beck, B.H., Kim, H.-G., Kim, H., Samuel, S., Liu, Z., Shrestha, R., Haines, H., Zinn, K., and Lopez, R.D. (2010). Adoptively transferred ex vivo expanded gammadelta-T cells mediate in vivo antitumor activity in preclinical mouse models of breast cancer. *Breast Cancer Res. Treat.* 122, 135–144.
36. Nicol, A.J., Tokuyama, H., Mattarollo, S.R., Hagi, T., Suzuki, K., Yokokawa, K., and Nieda, M. (2011). Clinical evaluation of autologous gamma delta T cell-based immunotherapy for metastatic solid tumours. *Br. J. Cancer* 105, 778–786.
37. Meidenbauer, N., Marienhagen, J., Laumer, M., Vogl, S., Heymann, J., Andreesen, R., and Mackensen, A. (2003). Survival and tumor localization of adoptively transferred Melan-A-specific T cells in melanoma patients. *J. Immunol.* 170, 2161–2169.
38. Bobisse, S., Rondina, M., Merlo, A., Tisato, V., Mandruzzato, S., Amendola, M., Naldini, L., Willemsen, R.A., Debets, R., Zanovello, P., and Rosato, A. (2009). Reprogramming T lymphocytes for melanoma adoptive immunotherapy by T-cell receptor gene transfer with lentiviral vectors. *Cancer Res.* 69, 9385–9394.
39. Ma, M.T., Meszaros, L.K., Paterson, B.M., Berry, D.J., Cooper, M.S., Ma, Y., Hider, R.C., and Blower, P.J. (2015). Tripodal tris(hydroxypyridinone) ligands for immuno-conjugate PET imaging with $(^{89}\text{Zr})^{4+}$: comparison with desferrioxamine-B. *Dalton Trans.* 44, 4884–4900.
40. Roullet, M., Gheith, S.M.F., Mauger, J., Junkins-Hopkins, J.M., and Choi, J.K. (2009). Percentage of $\gamma \delta$ T cells in panniculitis by paraffin immunohistochemical analysis. *Am. J. Clin. Pathol.* 131, 820–826.
41. Van Acker, H.H., Anguille, S., Willemsen, Y., Smits, E.L., and Van Tendeloo, V.F. (2016). Bisphosphonates for cancer treatment: Mechanisms of action and lessons from clinical trials. *Pharmacol. Ther.* 158, 24–40.
42. Prabhakar, U., Maeda, H., Jain, R.K., Sevick-Muraca, E.M., Zamboni, W., Farokhzad, O.C., Barry, S.T., Gabizon, A., Grodzinski, P., and Blakey, D.C. (2013). Challenges and key considerations of the enhanced permeability and retention effect for nano-medicine drug delivery in oncology. *Cancer Res.* 73, 2412–2417.
43. Hodgins, N.O., Al-Jamal, W.T., Wang, J.T.-W., Parente-Pereira, A.C., Liu, M., Maher, J., and Al-Jamal, K.T. (2016). In vitro potency, in vitro and in vivo efficacy of liposomal alendronate in combination with $\gamma \delta$ T cell immunotherapy in mice. *J. Control. Release* 241, 229–241.
44. Edmonds, S., Volpe, A., Shmeeda, H., Parente-Pereira, A.C., Radia, R., Baguña-Torres, J., Szanda, I., Severin, G.W., Livieratos, L., Blower, P.J., et al. (2016). Exploiting the Metal-Chelating Properties of the Drug Cargo for In Vivo Positron Emission Tomography Imaging of Liposomal Nanomedicines. *ACS Nano* 10, 10294–10307.
45. Dillman, R.O., Hurwitz, S.R., Schiltz, P.M., Barth, N.M., Beutel, L.D., Nayak, S.K., and O'Connor, A.A. (1997). Tumor localization by tumor infiltrating lymphocytes labeled with indium-111 in patients with metastatic renal cell carcinoma, melanoma, and colorectal cancer. *Cancer Biother. Radiopharm.* 12, 65–71.
46. Kershaw, M.H., Westwood, J.A., Parker, L.L., Wang, G., Eshhar, Z., Mavroukakis, S.A., White, D.E., Wunderlich, J.R., Canevari, S., Rogers-Freezer, L., et al. (2006). A phase I study on adoptive immunotherapy using gene-modified T cells for ovarian cancer. *Clin. Cancer Res.* 12, 6106–6115.
47. Ritchie, D.S., Neeson, P.J., Khot, A., Peinert, S., Tai, T., Tainton, K., Chen, K., Shin, M., Wall, D.M., Hönemann, D., et al. (2013). Persistence and efficacy of second generation CAR T cell against the LeY antigen in acute myeloid leukemia. *Mol. Ther.* 21, 2122–2129.
48. Botti, C., Negri, D.R., Seregini, E., Ramakrishna, V., Arienti, F., Maffioli, L., Lombardo, C., Bogni, A., Pascali, C., Crippa, F., et al. (1997). Comparison of three different methods for radiolabelling human activated T lymphocytes. *Eur. J. Nucl. Med.* 24, 497–504.
49. Griffith, K.D., Read, E.J., Carrasquillo, J.A., Carter, C.S., Yang, J.C., Fisher, B., Aebbersold, P., Packard, B.S., Yu, M.Y., and Rosenberg, S.A. (1989). In vivo distribution of adoptively transferred indium-111-labeled tumor infiltrating lymphocytes and peripheral blood lymphocytes in patients with metastatic melanoma. *J. Natl. Cancer Inst.* 81, 1709–1717.
50. Fruhwirth, G.O., Diocou, S., Blower, P.J., Ng, T., and Mullen, G.E.D. (2014). A whole-body dual-modality radionuclide optical strategy for preclinical imaging of metastasis and heterogeneous treatment response in different microenvironments. *J. Nucl. Med.* 55, 686–694.
51. Wang, Z., and Goonewardene, L.A. (2004). The use of MIXED models in the analysis of animal experiments with repeated measures data. *Can. J. Anim. Sci.* 84, 1–11.